Thermal and Kinematic Sunyaev-Z'eldovich Effects: Five Decades of Uncovering Relics

Submitted by Louis Penafiel

on 11 May 2020 in partial fulfillment of the requirements for the degree Master of Science in Physics at Cornell University

Cornell University, Ithaca, NY 14853, USA
Email: lap279@cornell.edu

Committee Members:

Dr. Michael Niemack (Chair)
Dr. Rachel Bean
Dr. Nicholas Battaglia

Contents

1 Introduction

The universe originally started hot and dense, during which photons were interacting with matter. As the universe expanded and cooled, the temperature dropped. Once it reached below $3,000$ K, when the universe was around 300,000 years old, atomic hydrogen formed, decoupling the photons from matter. These photons travelled freely throughout the universe, which continued to expand and cool, as a remnant that we can observe today as relic radiation, we call Cosmic Microwave Background (CMB).

Sunyaev and Z'eldovich theorized that perturbations in the matter density in a homogeneous and isotropic universe that allows for the formation of galaxies should have spatial fluctuations in the CMB (Sunyaev & Zeldovich, 1970). These manifest when the CMB photons interact with free, high energy electrons and lead to small spectral distortions in the CMB (Sunyaev & Zeldovich, 1972). The high energy portion is necessary, so that the electrons can transfer their kinetic energy to the CMB photons. These effects, which we know refer to as the SZ effects, were originally too small to detect, when the CMB was first discovered in the 1960s (Penzias & Wilson, 1965). However, with multiple decades of advancements in the experimental, observational, and theoretical fronts, much about the SZ effects have been elucidated.

There are multiple kinds of SZ effects: thermal, kinematic, relativistic, polarization, and non-thermal. The thermal SZ (tSZ) effect corresponds to scattering with the electrons from the ICM, while the kinematic SZ (kSZ) effect correspond to the electrons that move with large bulk velocities (Sunyaev & Zeldovich, 1970, 1972, 1980). Based on the speed of the electrons, relativistic corrections may need to be taken into account, hence the relativistic SZ effect (rSZ). There are also non-thermal contribution from turbulence and magnetic fields; we call these contributions the non-thermal SZ effect (ntSZ). Lastly, the scattering of CMB photons by free electrons inside clusters lead to a small polarization effect, hence polarized SZ effect (pSZ) (Mroczkowski et al., 2019b).

In this examination, we provide a literature review of the various SZ effects, specifically the tSZ and kSZ effects. Back in 2002, there was a literature review done by Carlstrom et al. (2002), which discussed past observations, but there have been decades of advancements, such as the first measurement of the pairwise kSZ signals (Hand et al., 2012), and various sky surveys. There was a more recent literature review on the SZ effects by Mroczkowski et al. (2019b), but this one focused more on how the SZ effects can help us understand the intracluster medium (ICM). This literature review hopes to further expand on what Mroczkowski et al. (2019b) have done by including how the SZ effects can also improve our understanding of large scale structure and cosmology, as well as go into details of how we extract the tSZ and kSZ signals.

We first provide a theoretical introduction to the SZ effects. We then move on to the motivations behind studying these effects, including their impact on galaxy clusters, large scale structure, and cosmology. After going into detail on various tSZ and kSZ extraction methods, we delve into the various types of observations and experiments done in the past. Then, we discuss current and future experiments and the promise that they hold.

Note: Nothing in this work represents original work, except for the compilation of the review itself.

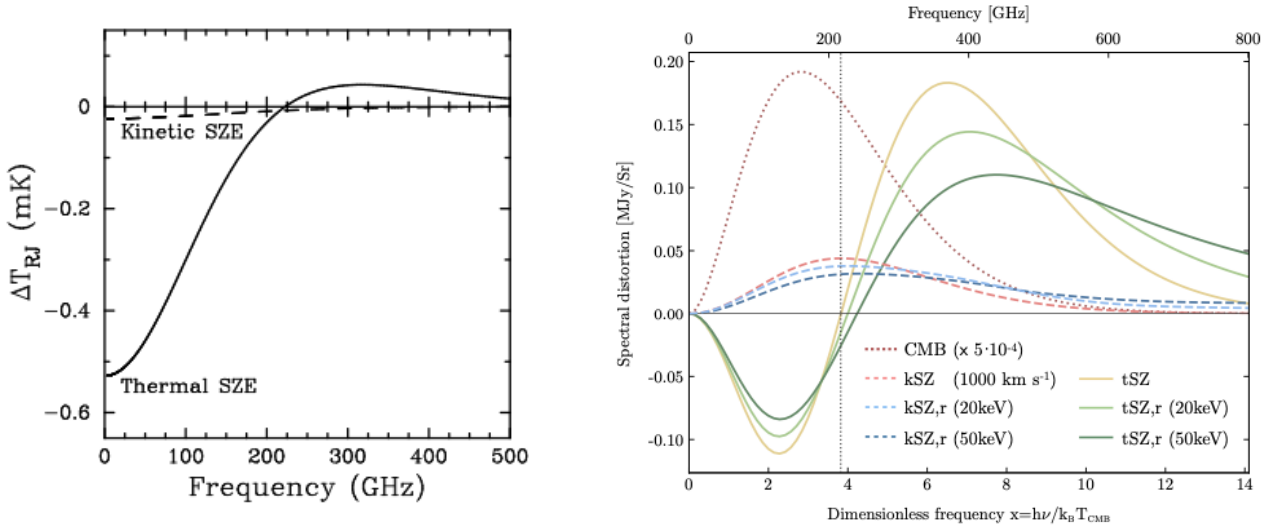

Figure 1: Spectral distortions caused by the various SZ effects in the CMB. *Left*: Shows the Rayleigh-Jeans brightness temperature with cluster properties electron temperature, T_e, of 10 keV, Compton-y parameter of 10^{-4}, and peculiar velocity of 500 km s^{-1}. Figure from Carlstrom et al. (2002). *Right*: Shows the intensity with an optical depth, τ_e of 10^{-2} and a Compton-y parameter of 10^{-4}. Figure from Mroczkowski et al. (2019b)

2 Thermal Sunyaev-Z'eldovich Effect

2.1 Theory

This subset of SZ effects focuses on those caused by hot electrons provided by the ICM of galaxy clusters. The interaction boosts the CMB photon energy, causing a small distortion ($\sim$ 1 mK) distortion in the CMB spectrum. From Fig. 4, the distortion appears as a decrement in the CMB at frequencies less than 218 GHz and an increment at the higher frequencies.

As follows is the derivation of the tSZ based on the original papers and reviews (e.g. (Carlstrom et al., 2002; Mroczkowski et al., 2019b; Sunyaev & Zeldovich, 1972)). Defining the dimensionless frequency as $x \equiv h\nu/k_B T_{CMB}$, the tSZ effect expressed as a temperature change ΔT_{tSZ} is given by

$$\frac{\Delta T_{tSZ}}{T_{CMB}} = f(x)y = f(x)\int n_e \frac{k_B T_e}{m_e c^2}\sigma_T d\ell = f(x)\frac{\sigma_T}{m_e c^2}\int P_e d\ell \tag{2.1}$$

where we used the equation for the pressure due to the electrons ($P_e = n_e k_B T_e$ in the last equivalence. y is the Compton-y parameter, which is equal to the optical depth, τ_e, multiplied by the fractional energy gained per scattering. σ_T is the Thompson cross-section, since in the non-relativistic limit, Compton scattering is simply Thompson scattering. n_e, T_e, and $m_e c^2$ are the number density, temperature, and rest energy of the electrons, respectively. Lastly, k_B is just the Boltzmann's constant and the integral is over the line of sight.

As seen in the above equation, the frequency dependence for the tSZ comes in the function f(x)

$$f(x) = \left(x\frac{e^x+1}{e^x-1} - 4\right)(1 + \delta_{tSZ}(x, T_e)) \tag{2.2}$$

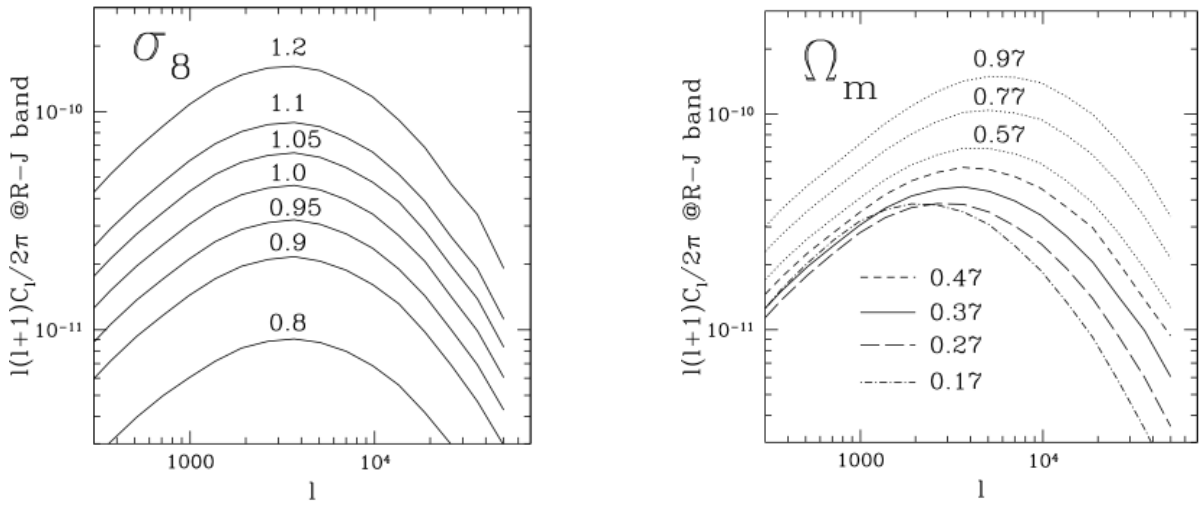

Figure 2: tSZ angular power spectra dependence on certain cosmological parameters. *Left*: Shows the σ_8 dependence Komatsu & Seljak (2002). *Right*: Shows the Ω_M dependence. Figures from Komatsu & Seljak (2002). **Note**: This paper assumes a flat universe and $w = -1.0$

where δ_{tSZ} is the relativistic correction to the frequency dependence, of which we do not account for in the tSZ in this review. Therefore, in the non-relativistic limit $f(x) \to 2$.

Taking the derivative of the blackbody with respect to the temperature, we can transform Δ_{tSZ} into units of specific intensity, which are common in mm and sub-mm tSZ observations, yielding

$$\Delta I_{tSZ} = g(x) I_0 y \tag{2.3}$$

where $I_0 = 2(k_B T_{CMB}^3/(hc)^2$ and the frequency dependence is given by

$$g(x) = \frac{x^4 e^x}{(e^x - 1)^2}\left(x\frac{e^x + 1}{e^x - 1} - 4\right)(1 + \delta_{tSZ}(x, T_e)). \tag{2.4}$$

2.2 Applications

There are several features that make the tSZ relevant for finding clusters and understanding the evolution of the universe including:

- independence in redshift
- unique and small ($\sim$ 1 mK) spectral signature compared to the CMB
- integrated tSZ flux is proportional to the total thermal energy of the cluster (Carlstrom et al., 2002).

Because of these features, the last of which is discussed, as in (Carlstrom et al., 2002), right after, we can extract cosmological parameters of which are discussed in Appendix A. The integrated tSZ signal, Y_{SZ} is relevant for finding clusters. Integrating the tSZ over the solid angle of the cluster, $d\Omega = dA/D_A^2$ yields

$$Y_{SZ} = \int \Delta T_{tSZ} d\Omega \propto \frac{N_e \langle T_e \rangle}{D_A^2} \propto \frac{M \langle T_e \rangle}{D_A^2} \tag{2.5}$$

where $\langle T_e \rangle$ is the mean electron temperature, M is the mass of the cluster, D_A is the angular diameter distance, and N_e is the total number of electrons in the clusters.

Hubble constant, H: For the Hubble constant, we use the relations for the tSZ and X-ray emissions to the density, $\Delta T_{tSZ} \propto \int D_A d\zeta n_e T_e$ and $S_x \propto \int D_A d\zeta n_e^2 \Lambda_{eH}$, where Λ_{eH} is the X-ray cooling function, respectively. Combining these two relations, we get

$$D_A \propto \frac{(\Delta T_0)^2 \Lambda_{eH0}}{S_{x0} T_{e0}^2} \frac{1}{\theta_c} \tag{2.6}$$

where the subscript 0 means we took the integral along the line of sight through the center of the cluster and θ_c is the characteristic scale of the cluster along the line of sight.

Since measurements only yield the characteristic scale of the cluster in the plane of the sky, various relations are needed to relate the line of sight and plane of sky scales, which are discussed in various papers (Birkinshaw & Hughes, 1994; Reese et al., 2000). Once we make that calculation, we can combine this with the redshift of the cluster along with the geometry of the universe to determine the Hubble parameter. This yields an independent measurement, making it a valuable check of distance determinations of the universe, like a multi-tracer approach to the type Ia supernova measurements (Perlmutter et al., 1999).

Matter abundance, Ω_M: Most of the baryons contained in the ICM are confined to the cluster potential, so there is around an order of magnitude more baryonic mass in the ICM compared to observations in the galaxies themselves, (White et al., 1993). Hence, the cluster baryonic mass fraction is a reasonable approximation to the universal baryon mass fraction, f_B. A measurement of f_B with a determination of Ω_B can lead to a direct estimate of Ω_M because of the definition, $f_B \equiv \Omega_B/\Omega_M$. This measurement can be compared to measurements done by analyses of BBN predictions done with uncertainty propagation (e.g. Burles et al. (2001)) and Deuterium measurements in Lyman α forests (e.g. Burles & Tytler (1998)), as well as those done by CMB measurements (Aghanim et al., 2016a; Pryke et al., 2002).

Furthermore, as seen in Fig. 2, once you obtain the tSZ angular power spectra, one can place constraints on Ω_M because of the strong dependence.

RMS density fluctuations, σ_8: Again from inspecting Fig.2, one can place constraints on σ_8, by getting a tSZ angular power spectra.
Optical depth, τ_e: Lastly because of the explicit dependence on the optical depth of tSZ allows for τ's measurement (e.g. Sehgal et al. (2005)). This gives an independent measurement to the one calculated using pairwise statistics of the kSZ (discussed later), as seen in Bernardis et al. (2017) by using data from the Atacama Cosmology Telescope Polarimeter (ACTPol) and Baryon Oscillation Spectroscopic Survey (BOSS) DR11 (Font-Ribera et al., 2013).

The focus from applications to cosmology shifted to ICM astrophysics, when the main contribution to the tSZ power spectrum came from low-mass groups and clusters, which was in contrast of the original prediction of tSZ power spectrum dominated by massive clusters at intermediate redshifts Cole & Kaiser (1988); Shaw et al. (2010). Furthermore, Y_{SZ} is proportional to thermal energy content of the ICM. Combining the tSZ power spectrum with data of cosmological parameters and X-ray measurements from other probes, makes it a powerful tool to constrain ICM

astrophysics (Mroczkowski et al., 2019b).

Shock Fronts: Galaxy cluster mergers are some of the most energetic processes in the universe, and a large fraction of that energy is dissipated as shock that heats the ICM (McCarthy et al., 2007). These shock fronts should be observable in the high spatial resolution tSZ measurements as a pressure jump (Markevitch & Vikhlinin, 2007; Ruan et al., 2013). tSZ is advantageous in studying shocks because of its redshift independence and linear dependence on gas density, allowing for a wider breadth of observations compared to X-ray satellites. High sensitivity and high angular resolution are required to study shocks, which have been done with previous experiments.

Pressure Substructure: With high enough angular resolution imaging, it can be possible to detect pressure substructures in the ICM. These substructures are related to the tSZ as the gas compression in merger events are associated to infalling subsructures in the ICM. Understanding the underlying ICM physics will be aided by tSZ substructure characterization (Mroczkowski et al., 2019b).

Lastly, the tSZ can test galaxy models Mroczkowski et al. (2019a). The effects of feedback leave an imprint on the tSZ profile that are observable in a large statistical samples (Croton et al., 2006). These measurements can constrain how cosmological simulations describe galaxy formation and AGN feedback (Battaglia et al., 2019).

2.3 Extraction

The extraction method that yields the best S/N is through filtering the map using a matched filter. We discuss below the matched filter approach taken by Hasselfield et al. (2013), which is based on the Universal Pressure Profile, theorized by Arnaud et al. (2010).

The pressure is modeled after a generalized Navarro-Frenk-White (GNFW) profile, explicitly, the electron pressure is

$$P(r) = P_{500}\left(\frac{M_{500}}{3\times10^{14}M_{\odot}}\right)^{\alpha_p} p(x) \tag{2.7}$$

where

$$P_{500} = 1.65\times10^{-3}E(z)^{8/3}\left(\frac{M_{500}}{3\times10^{14}M_{\odot}}\right)\text{keV cm}^{-3}., \tag{2.8}$$

$$p(x) = P_0(c_{500}x)^{-\gamma}(1+(c_{500}x)^{\alpha})^{(\gamma-\beta)/\alpha} \tag{2.9}$$

with $E(z)$ is the ratio of the Hubble constant at redshift z compared to its present value and the following best fit values, $\alpha_p = 0.12+\alpha_p'(x)$ and $\{P_0, c_{500}, \gamma, \alpha, \beta\} = \{8.403h_{70}^{3/2}, 1.177, 0.3081, 1.0510, 5.4905\}$

For this specific pressure profile and ignoring relativistic effects, the Compton-y parameter as a function of θ becomes

$$y(\theta) \propto \int dsP(\sqrt{s^2+(R_{500}\theta/\theta_{500})^2}) \tag{2.10}$$

where $\theta_{500} = R_{500}/D_A(z)$ and $D_A(z)$ is the angular diameter to redshift z.

Then, combining the above expressions, Hasselfield et al. (2013), finds the following relation

$$y(\theta, m) \approx 10^{A_0} E(z)^2 m^{1+B_0} \tau(m^{C_0}\theta/\theta_{500}) \tag{2.11}$$

with fiducial values $\{10^{A_0}, B_0, C_0\} = \{4.950 \times 10^{-5} h_{70}^{1/2}, 0.08, = -0.025\}$ and $m \equiv M_{500c}/(3 \times 10^{14} h_{70}^{-1} M_\odot)$.

After finding the optical depth, a set of matched filters, based on the optical depth profile, are made, i.e. $S_{\theta_{500}}(\theta) \equiv \tau(\theta/\theta_{500})$. For each signal template, the associated matched filter in Fourier space is

$$\Psi_{\theta_{500}} = \frac{1}{\Sigma_{\theta_{500}}} \frac{B(\mathbf{k}) S_{\theta_{500}}(k)}{N(\mathbf{k})} \tag{2.12}$$

where $B(\mathbf{k})$ is the telescope beam response multiplied with the map pixel window function, $N(\mathbf{k})$ is the anisotropic noise power spectrum of the map, and $\Sigma_{\theta_{500}}$ is a normalization factor. This normalization is chosen such that when applied to a map that contains a beam-convolved cluster signal, the output of the matched filter returns the central tSZ temperature decrement $-\Delta T_{tSZ}$, as wanted.

3 Kinematic Sunyaev-Z'eldovich Effect

3.1 Theory

Now, we consider the kSZ, which comes from the bulk motion of the cluster and the corresponding Doppler effect when those electrons scatter with CMB photons. If the cluster velocity has a component along the line of sight to the cluster, then this will manifest into an observed distortion to the CMB spectrum.

Since the velocity distribution is anisotropic, actually mono-diretional, when averaging over all scattering angles of the photons, a linear order Doppler term remains (Mroczkowski et al., 2019b). This distortion, in the non-relativistic limit, is given by Sunyaev & Zeldovich (1980),

$$\frac{\Delta T_{kSZ}}{T_{CMB}} = -\int d\ell \sigma_T n_e \frac{\mathbf{v_{pec}} \cdot \hat{r}}{c} = -\tau_e \left(\frac{v_{pec}}{c}\right) \tag{3.1}$$

where v_{pec} is along the line of sight.

3.2 Applications

On small enough scales, mutual gravitational attraction causes clusters of galaxies to move towards each other. Therefore, a measurement of this pairwise motion can be a valuable consistency check for the standard cosmological model(Flender et al., 2016). In the PoV of the observer, a cluster pair would have opposite line-of-sight (LOS) velocities. The average velocity at which clusters at a given distance move towards each other (pairwise velocity of clusters) can be estimated using only information about their LOS velocities (Ferreira et al., 1999). However, these peculiar velocities

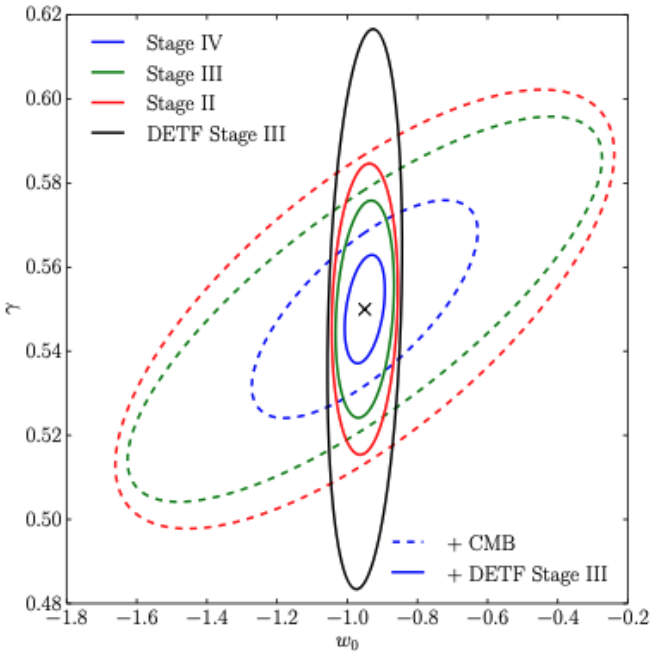

Figure 3: 2D projected likelihoods for the w_0 and γ parameters. Lines correspond to future surveys. Figure from Mueller et al. (2015b)

themselves are difficult to measure, since they require extremely precise measurements of redshifts and distances. Because of the relationship between the kSZ and v_{pec}, they can be a potential probe of the clusters' LOS peculiar velocities, and hence a probe for extensions to the standard cosmological model. Also, like the tSZ, they can also probe ICM substructure.

Cosmological Models: The peculiar velocities of clusters provide an alternative and independent measurement of the cosmological gravitational potential field (Mueller et al., 2015b). Therefore, measuring the pairwise kSZ can provide a powerful complementary measurement of gravity's influence on cosmic structure (DeDeo et al., 2005). Since, Mueller et al. (2015b) aimed to constrain dark energy and cosmic modifications to gravity, then a measurement of the pairwise kSZ signal can place constraints on γ and w_0, as seen in Fig. 3. These uncertainties were found using the Fisher matrix formalism as described in Appendix B.

Massive neutrinos: By extending the ΛCDM parameter space to include massive neutrinos, these in turn can be probed by combining the pairwise kSZ measurements with Planck primordial CMB priors and place constraints on sums of neutrino masses (Mueller et al., 2015a).

ICM Substructures: In principle, maps of kSZ signal can measure internal gas motions in the ICM (Cooray & Chen, 2002; Nagai et al., 2003; Sunyaev et al., 2003). They will provide a complementary measure of the gas motions to those from measurements done in X-ray analyses.

Missing Baryons: A cosmic web of filaments is essential for large-volume cosmological simulations, and should be found at temperatures $10^5 - 10^7$ K (Cen & Ostriker, 2006; Shull et al., 2012). The gas is too warm to be detected in active galactic nuclei, but too soft to be observed in X-rays (Bregman et al., 2009; Nicastro et al., 2008). Because the kSZ signal directly traces the distribu-

tion of baryons in the circumgalactic medium, they can probe the thermodynamic properties of it.

Reionization: Reionization left imprints on the CMB, which can be observed in the kSZ power spectrum from the epoch of reionization and from the ICM, galaxies, and clusters Battaglia et al. (2013).

3.3 Extraction

Because the signal for single clusters is challenging, due to its small amplitude ($\mathcal{O} \sim \mu K$) and degenerate spectral dependence, it is more practical to measure the pairwise motion of clusters. There are multiple ways to extract information about kSZ signal. We expand upon the Aperture Photometry (AP) method for the pairwise kSZ signal as done in Calafut et al. (2017). AP isolates the kSZ signal from the CMB by necessitating that the kSZ to be localized in the cluster and that the CMB to be correlated over long wavelengths. This is so that when we take the difference, we remove the CMB contribution, while keeping the kSZ contribution intact. Specifically, the AP temperature is the difference between the average CMB pixel temperature within a given angular radius Θ, which is comparable to the cluster size, and CMB pixel temperature within an annulus, outside the radius of width $\sqrt{2}\Theta$[1], i.e. $T_{AP} = \langle T_{inner} \rangle - \langle T_{annul} \rangle$.

The kSZ temperature is then given by

$$\Delta T_i = T_{AP} - \bar{T}_{AP} \tag{3.2}$$

where T_{AP} corresponds to the kSZ amplitude estimated from AP, and $\bar{T}_{AP}$ is the averaged aperture temperature over all cluster locations as done in Hand et al. (2012), which takes into account possible redshift evolution of the tSZ sources and is given by

$$\bar{T}_{AP} = \frac{\Sigma_j T_{AP} \exp\left(- \frac{(z_i - z_j)^2}{2\sigma_z^2} \right)}{\Sigma_j \exp\left(- \frac{(z_i - z_j)^2}{2\sigma_z^2} \right)} \tag{3.3}$$

where the sum is over all galaxies in the same redshift bin, where $j \neq i$.

A measure of gravitationally infalling clusters show up in the correlation of cluster velocities because the kSZ signal is a direct measure of the cluster momentum. This shows up in the related kSZ signal in the CMB. These peculiar velocity correlations are obtained by employing the pairwise estimator, described in Hand et al. (2012),

$$\hat{p}_{kSZ}(r) = -\frac{\Sigma_{i<j}(\Delta T_i - \Delta T_k) c_{ij}}{\Sigma_{i<j} c_{ij}^2} \tag{3.4}$$

where the sum is over all cluster pairs, located at positions $\mathbf{r}_{i,j} = \hat{r}_{i,j}, z_{i,j}$ that are separated by a distance r = $|\mathbf{r}_{ij}| = |\mathbf{r}_i - \mathbf{r}_j|$. The ΔT_i is the kSZ temperature increment/decrement at the ith cluster location. The weights are calculated to be

[1]This coefficient does not have to be $\sqrt{2}$, as long as it's appropriate in cancelling out the CMB temperature

$$c_{ij} = \hat{r}_{ij} \cdot \frac{\hat{r}_i + \hat{r}_j}{2} = \frac{(r_i - r_j)(1 + \cos\alpha)}{2\sqrt{r_i^2 + r_j^2 - 2r_i r_j \cos\alpha}} \tag{3.5}$$

where α is the angle between $\hat{r}_i$ and $\hat{r}_j$.

Other extraction methods include using the cross-correlation of the CMB map with a velocity field, which has been constructed from the position of galaxies with linear perturbation theory (Schaan et al., 2015). Another approach is using the square of CMB anisotropy maps (Ferraro et al., 2016; Hill et al., 2016).

4 Previous observations

4.1 tSZ History

4.1.1 Single Dish Telescopes

From Fig. 4, the largest temperature distortion corresponds to measuring the tSZ decrement on the lower end of the GHz frequencies. Hence, the first attempts to measure the tSZ were focused on the decrement by using single dish telescopes near 15 GHz (Birkinshaw et al., 1978; Gull & Northover, 1976). Then, in the mid-1980s, the Owens Valley Radio Observatory (OVRO) 40-meter provided more reliable detections as it had on the order of tens of hours of integration time (Birkinshaw et al., 1984). In the 90s, advancements in photometric instruments, such as bolometers, were used to focus single dish telescopes on the 150 GHz frequency, where the tSZ decrement is the strongest. Such experiments include Sunyaev-Z'eldovich Infrared Experiment (SuZIE) and Diabolo (Désert et al., 1998; Wilbanks et al., 1994).

After advancements in technology, focus moved towards measuring the SZ increment. The first measurement was done by focusing on cluster A2163 on the PRONAOS balloon experiment at 350 GHz; the first spectro-photometric measurement of the SZ spectrum was done by combining this data with the Diabolo and SuZIE measurements (Lamarre et al., 1998). Then, using the Submillimeter Common-User Bolometer Array (SCUBA) on the James Clerk Maxwell Telescope (JCMT), which also focused at 350 GHz, Komatsu et al. (1999), gave the first successful imaging of the SZ increment. Then, with the use of Large Apex Bolometer Camera (LABOCA) on APEX-SZ on the same cluster gave higher-quality SZ increment images (Nord et al., 2009). Then, more SCUBA observations allowed for the first large statistical study of the increment (Zemcov et al., 2007).

Now, the focus shifted to studying the entire spectrum of the tSZ, not just the increment or the decrement. With the Herschel-SPIRE photometer, Zemcov et al. (2010) mapped several bands as part of the Herschel Lensing Survey (HLS) and performed the first detection of the tSZ for > 600 GHz. Then the first high-resolution SZ spectral measurement was done using the Z-spec instrument, by focusing towards the cluster RX J1347. 5-1145 (Zemcov et al., 2012); the results of which are shown in Fig. 4. The following multi-band photometric measurements focused on MACS J0717. 5+3745 because of its high velocity, ultimately yielding a low-significance indication of a non-zero kSZ signal (Adam et al., 2017; Mroczkowski et al., 2012; Sayers et al., 2013).

Another significant improvement came in the angular resolution with the use of the Multiplexed SQUID/TEC Array at Ninety Gigahertz (MUSTANG) Camera on the 100-m Green Bank Telescope (GBT), which allowed for the imaging of shock and pressure substructures in a handful of clusters (Dicker et al., 2008; Korngut et al., 2011; Mason et al., 2010).

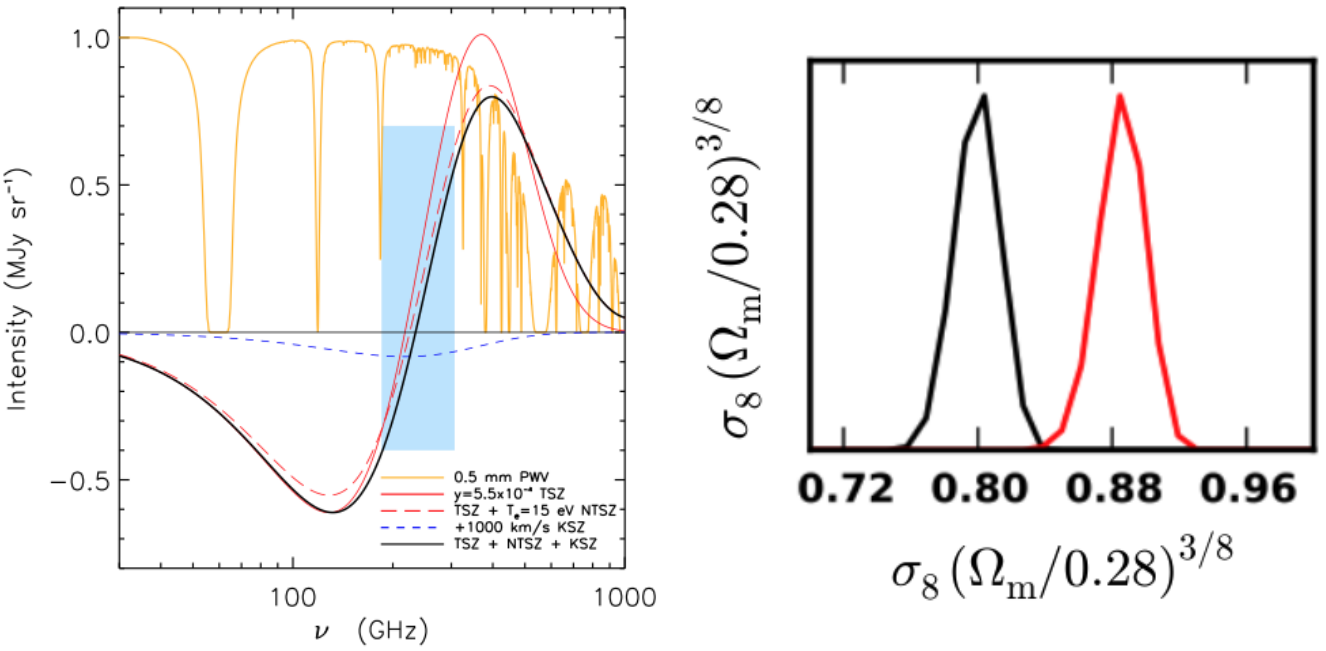

Figure 4: tSZ measurements and constraints *Left*: The first high resolution SZ spectral measurement from the Zspec instrument. SZ effects from 30 to 1000 GHz. Figure from (Zemcov et al., 2012) *Right*: σ_8 constraints based on Planck observations. The red and black lines correspond to a mass bias of 0.2 and 0.4, respectively. Figure from Aghanim et al. (2016b).

4.1.2 Interferometers

Now make an array with these single dish telescopes, we can then combine these signals, essentially making a larger antenna and improving the resolution, without the requirement of building large aperture elements. The stability comes from its ability to perform simultaneous differential sky measurements over defined spatial frequencies, by measuring the time average correlation of the signals from pairs of telescopes (Richard Thompson et al., 2017).

Furthermore, the uncorrelated atmospheric signal is naturally filtered, but it comes at the expense that the data behaves as a frequency-dependent spatial filter (i.e. not as sensitive) and low mapping speed, compared to a single dish. These interferometric observations were first performed at the Very Large Array (VLA) (Moffet & Birkinshaw, 1989) and the Ryle Telescope (Jones et al., 1993). These two, in turn, provided the first SZ imaging and detection of the decrement solely on the signal.

The OVRO 10-m array and Berkeley-Illinois-Maryland Array (BIMA) in the 90s, and the Sunyaev-Zeldovich Array (SZA) and the Combined Array for mm-wave Astronomy (CARMA) in the 2000s pushed these measurements further up to 90 GHz (e.g. Carlstrom et al. (1996)). They also obtained a 20" resolution images of an offset in the SZ centroid, but since it was not analyzed in detail, it was used for determinations of the angular diameter distance Reese et al. (2002).

4.1.3 Surveys

Focus then moved on to make maps/surveys of the SZ signal to allow for the study of the growth of structure as well as have probes of cosmology, such as those discussed in the above section. The first high spatial resolution SZ images came from the IRAM 30-m telescope and the NRO 45-m telescope at RX J1347. 5-1145, ultimately delivering a 5' × 5' and 2' × 2' map, with 20" and

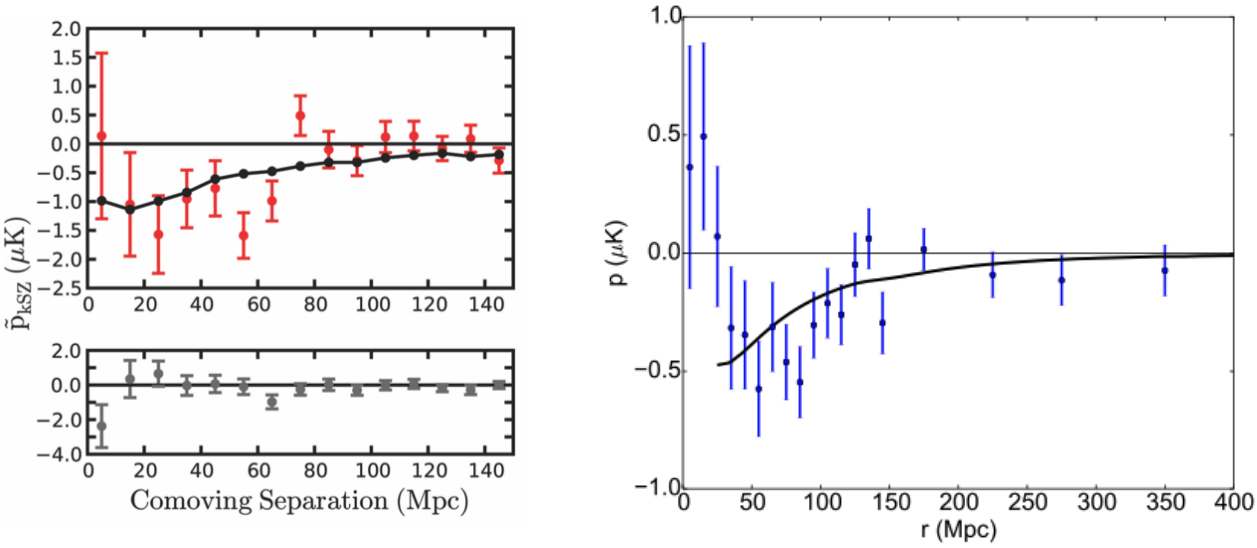

Figure 5: Pairwise momentum estimator from the pairwise kSZ signal *Left*: Shows the mean pairwise momentum estimator for the 5000 most luminous BOSS DR9 galaxies within ACT. Figure from Hand et al. (2012). *Right*: Shows the mean pairwise momentum estimator from the 9800 most luminous DR11 galaxies in the ACT region. Figure from Bernardis et al. (2017)

13" resolution, respectively (Komatsu et al., 1999, 2001; Pointecouteau et al., 1999). These maps exhibited an excess SZ signal, which was later confirmed by Chandra (Allen et al., 2001).

Improvements in photometric imaging arrays, such as the Atacama Pathfinder Experiment Sunyaev-Zeldovich Experiment (APEX-SZ), large statistical samples of cluster images were done using single dish measurement (Schwan et al., 2003). Then, these measurements were performed over clusters to image larger statistical samples with the Arcminute MicroKelvin Interferometer (AMI) and the Array for Microwave Background Anisotropy (AMiBA) (e.g. Lin et al. (2009); Muchovej et al. (2007)).

Around a decade ago, the South Pole Telescope (SPT) and the Atacama Cosmology Telescope (ACT), achieved high mapping speeds to allow for wide-field surveys based on their tSZ signals (Menanteau et al., 2010; Staniszewski et al., 2009). Complementing these ground-based surveys, the Planck satellite delivered a catalogue of roughly 2000 SZ clusters (Ade et al., 2016b). Because of its 9 photometric bands, spanning from 30-850 GHz, Planck data was gives the broadest frequency coverage of the SZ spectrum to date (Hurier, 2016). Furthermore, its measurements of the tSZ spectrum has allowed bounds to be placed on cosmological parameters, including σ_8 as seen in Fig. 4. Shocks were also studied near the Coma Cluster (Ade et al., 2013). Also, Planck data provided the first possible detection of the cosmic web, using the tSZ effect (Tanimura et al., 2019; de Graaff et al., 2019). From these analyses, a significant fraction of the missing baryons are recovered.

4.2 kSZ History

Hand et al. (2012) combined the high resolution CMB data from the ACT and the Baryon Oscillation Spectroscopic Survey (BOSS) spectroscopic catalog (Ahn et al., 2012), as seen in Fig. 5, providing the first detection of the pairwise kSZ signal. Subsequent detections were found in Planck CMB data, in conjunction with the Central Galaxy Catalog from the Sloan Digital Sky Survey (SDSS) with a statistical significance of $1.8 - 2.5\sigma$ (Abazajian et al., 2009; Ade et al., 2016a).

Higher significance detection of the pairwise kSZ signal is expected by combining SPT CMB data with the galaxy cluster catalog from the Dark Energy Survey (Carlstrom et al., 2011; Keisler & Schmidt, 2013). This was done by Soergel et al. (2016) and reported a 4.2σ significance. These measurements were subsequently expanded on by Bernardis et al. (2017) by combining ACTPol data with the BOSS DR11 data, with a 4.1σ significance, shown in Fig. 5.

Using the alternative approach of using a velocity reconstruction approach as prescribed by Schaan et al. (2015), this analysis reported a $2.9 - 3.3\sigma$ evidence of the kSZ using ACTPol data with velocity fields reconstructed from the BOSS DR10 catalog (Ahn et al., 2014). Ade et al. (2016a) also reported a detection of kSZ signal using Planck data with a statistical significance of $3.0 - 3.7\sigma$.

With the projected field approach, multi-frequency CMB maps from Planck and WMAP were cross-correlated wit the Wide-field Infrared Survey Explorer (WISE) galaxy measurements, yielding a $3.8 - 4.5\sigma$ significance for the kSZ signal (Ferraro et al., 2016; Hill et al., 2016).

5 Current and future experiments and promises

5.1 Current experiments

ALMA: Upgrades to the Atacama Large Millimeter/Submillimeter Array (ALMA) in the next few years include 2 bands covering $35 - 90$ GHz, which are frequencies best suited for probing the tSZ Kitayama et al. (2016). Because of the larger FoV and the ability to image a target in multiple array configurations at the same frequencies, will further improve our sensitivities to pressure substructures and shocks with the tSZ.

MUSTANG-2: The 2nd generation MUSTANG (MUSTANG-2) will replace MUSTANG-1 on the GBT(Dicker et al., 2014). Because of its window focused at 90 GHz, it will be used primarily for probing the tSZ decrement. Furthermore, it has one of the highest resolution bolometer cameras to probe the tSZ at 9" resolution

NIKA2: New IRAM Kid Arrays 2 (NIKA2) uses a mm camera, consisting of kinetic inductance detectors (KIDs) operating at 150 mK (Adam et al., 2018). Installed at the IRAM 30-m telescope, it can yield high-resolution SZ observations because:

- dual-band camera for which the tSZ is negative on one, and positive for the other
- 260 GHz map to detect point sources
- high angular resolution and large FoV.

5.2 Future experiments

TolTEC: The Large Millimeter Wave Telescope (LMT) 50 m at Sierra Negra, Mexico looks to install TolTEC, a new mm wave camera, in the coming year (Bryan et al., 2018). This camera will have filter passbands centered at 150, 220, and 280 GHz, spanning the peak in the kSZ.

CCAT-prime: CCAT-prime will be expected to begin its operations in 2021, and will have a 6-m aperture sub-mm telescope (Stacey et al., 2018). The bolometer camera in this telescope, Prime-Cam, covers the range between 190 and 450 GHz, which should have at least an order of magnitude improvements over the Planck data (Erler et al., 2018). Data combined with CMB surveys should

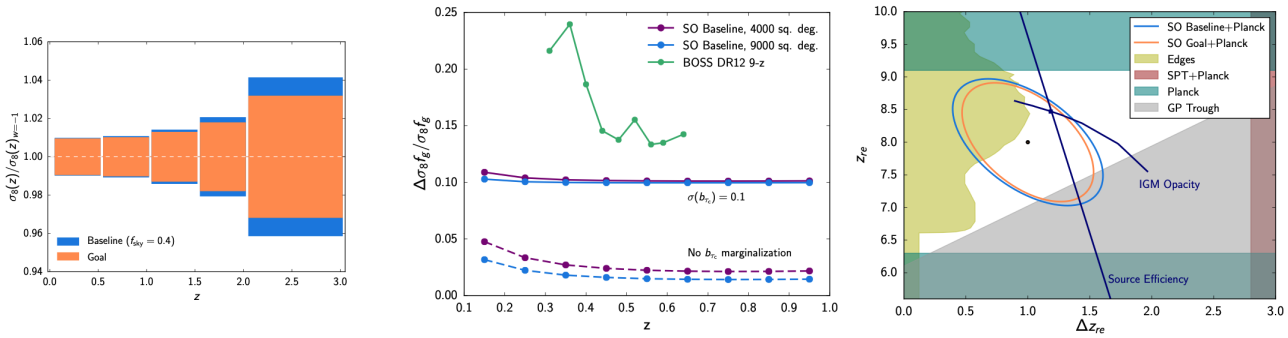

Figure 6: Various forecasts and predictions for the upcoming Simons Observatory *Left*: The uncertainty on σ_8 from abundances of SO-detected SZ clusters. *Middle*: Predictions from pairwise kSZ measurements from SO clusters on the logarithmic growth rate for large scale structure. *Right*: Summary and forecasts of constraints on the redshift and duration of reionization. Figures from Ade et al. (2016a)

facilitate the separation of tSZ and kSZ maps (Erler et al., 2018).

ACTPol and SPT-3G: Various instruments on the ACT and SPT will allow them to detect thousands of SZ selected clusters (Benson et al., 2014; Henderson et al., 2016).

SO:The Simons Observatory (SO) plans on combining several CMB experiments at the Atacama desert with CCAT-prime (Ade et al., 2019). SO aims to deliver strong constraints on the kSZ effect, as well as the ability to separate SZ components from each other, and should have first light in 2021. Examples of forecasts, which are calculated using Fisher matrices, as described in Appendix B, are given at Fig. 6.

CMB-S4: Specifications for CMB-Stage 4 (CMB-S4) are still being determined, but it will likely have a similar design to SO, with an anticipated start date in 2028 (Abazajian et al., 2016). The main improvements for this comes in detector count, which should be a couple orders of magnitude larger than SO.

AtLAST: The Atacama Large Aperture Submm/mm Telescope (AtLAST) aims to build a 50 m single dish observatory (Bertoldi, 2018). It primarily serves as a complement to the lower-resolution CMB primary anisotropies and SZ survey telescopes and probe higher contamination from dusty sources and the tSZ increment.

CSST:The Chajnator Sub/millimeter Survey Telescope (CSST) plans on building an inexpensive 30 m single dish survey telescope based between 90-420 GHz, based on the design by Padin (2014). They would provide extremely deep SZ maps for a large sample of clusters, while expanding spectral coverage and providing better angular resolution.

Vera C. Rubin Observatory, formerly LSST: This experiment allows for the measurement of high-redshift samples, due to a large increase in S/N (Ivezić et al., 2019). We can use the telescope's measurements of the non-linear regime through weak lensing, as a probe for the uncertainty in the impact of cosmological parameters and physical processes governing baryons (Kilbinger, 2015). This can improve our understanding on feedback efficiency (Battaglia et al., 2019)

Space missions: Future CMB mission concepts such as Cosmic Origins Explorer (COrE) (Delabrouille et al., 2018; Remazeilles et al., 2018) and Probe of Inflation and Cosmic Origins (PICO) (Sutin et al., 2018) could enable an increase in the number of detected SZ clusters, allowing vast numbers of cross-correlation studies. Another concept focuses on subarcminute angular resolution with the Millimetron Space Observatory (MSO) (Smirnov et al., 2012), by reconstructing cluster profiles of individual clusters.

6 Conclusion

Advancements in technology, observations, and theories have made substantial progress, since Sunyaev and Z'eldovich first theorized the SZ effects back in 1970. From first detection of the tSZ decrement to wide-field surveys, progress will only continue with the upcoming multi-band experiments, that probe a larger spectrum for 30 GHz to 1 THz), and the improved higher resolutions, both angular and spatial. These subsequent high resolution measurements can allow us to not only probe the standard cosmological model, but also finer properties of the ICM.

Further improvements to surveys, focusing on improving detectors, will allow us to probe more clusters and allow for more kSZ detections in cross-correlation studies, allowing us to place constraints on cosmological models and gas motions. However, with these improvements to the small kSZ signal, astrophysical contaminants, that are not discussed in this review, become prevalent.

Lastly, the other SZ effects, specifically the rSZ and the ntSZ, are within reach, due to the increase in resolution and sample sizes. These make the next decade of SZ effect measurements particularly exciting in several avenues from the cosmological sales to galaxy scales.

Acknowledgments

I would like to thank the members of this A Exam committee: Michael Niemack (who expanded on the original topic and serves as the committee chair), Rachel Bean (who originally proposed the topic of kSZ), and Nicholas Battaglia.

I would also like to thank Kacey Aquiliano and Craig Wiggers for their conversations regarding future career paths. I thank my cohort, especially the denizens of the party office: Benjamin Gregory, Eric San, Andrew Gomes, Vaibhav Sharma, Gaurav Gyawali, Avinash Mandaiya, and my housemate Chad Pennington (Cameron Flynn and Michael Kaemingk were part of it for a while), for their amazing physics and non-physics conversations, which make me realize that I'm going to miss academia. I also thank Rachel Bean for being my potential advisor in the fall semester.

I thank my various friends from college, high school, and middle school, as well as family and friends for their continued support and advice for my decision in taking a terminal Master's. I thank Aptima Inc. , who after an incredibly stressful, depressing, degrading four-month long job hunt, with open arms, were impressed by my work and hired me as an Associate Research Engineer, starting in June.

I want to thank my family, who immigrated from the Philippines when I was younger, to give me the life that I definitely (physics and engineering were not in my radar growing up) would not have had had we stayed, and supportive of my career. I hope that I can emulate them in the future with my sister.

Lastly, I want to thank my partner, Barbara Skrzypek, who without her continual support, would have not made any of this possible.

A Cosmological Parameters

The cosmological model that Mueller et al. (2015b) considered consisted of 9 parameters:

- $\Omega_b h^2$: baryon density
- $\Omega_M h^2$: matter density
- Ω_k: curvature density
- Ω_Λ: dark energy density
- w_0: present value of the dark energy equation of state
- w_1: rate of change of the dark energy equation of state
- n_s: spectral index of the primordial spectrum of curvature perturbations
- $\ln A_s$: normalization of the primordial spectrum of curvature perturbations
- γ: growth rate exponent, such that $f_g = \Omega_m(a)^\gamma$

where h is the Hubble constant and the fiducial parameters used in the mentioned analysis are $\{\Omega_b h^2, \Omega_M h^2, \Omega_k, \Omega_\Lambda, w_0, w_a, n_s, \ln A_s, \gamma\} = \{0.021805, 0.1225, 0, 0.75, -0.95, 0, 1, 3.1954, \text{chosen}\}$.

Other variables considered when constraining cosmological parameters include the mass density of neutrinos, Ω_ν, such that $\Omega_M = \Omega_{CDM} + \Omega_b + \Omega_\nu$, where CDM stands for cold dark matter. Ω_{CDM} is also another parameter to consider. Lastly, an important one is σ_8, the normalization of the CDM power spectrum in terms of RMS density fluctuations in spheres of radius $8h^{-1}$ Mpc, i.e. amplitude of matter fluctuations.

B Fisher Matrix Formalism

This portion is based on Wittman (20xx)'s treatment of Fisher matrices, which are in turn based on the formalism presented at Albrecht et al. (2006).

Consider a case where we have two observables, n_1 and n_2, which each have measurement uncertainty, σ_1 and σ_2. Furthermore, we only have two model parameters, pair production rate, α and 2-production only rate (β), so the model reads us

$$n_1 = \alpha + \beta \tag{B.1}$$
$$n_2 = \alpha \tag{B.2}$$

If we happen to overestimate or underestimate our measurements, thee will be a nonzero covariance between our estimates of the two parameters. This is where Fisher matrices come in handy because you only need to know your model and your measurement uncertainties to find these covariances. This is because the covariance matrix is the inverse of the Fisher matrix, which in turn, places constraints on the uncertainty of our model parameters because the Fisher matrix is the best possible we can do from the information content of the experiment.

In general, for N model parameters, $p_1, p_2, \ldots p_N$, the Fisher matrix F is an $N \times N$ symmetric matrix. Because each parameter involves a sum over the observables, and assuming we have B observables, $f_1, f_2, \ldots f_B$, then the elements of the Fisher matrix are

$$F_{jk} = \sum_b \frac{1}{\sigma_b^2} \frac{\partial f_b}{\partial p_j} \frac{\partial f_b}{\partial p_k} \tag{B.3}$$

From the above simple 2 observable, 2 parameter scenario, the Fisher matrix becomes

$$F = \begin{pmatrix} \frac{1}{\sigma_1^2} + \frac{1}{\sigma_2^2} & \frac{1}{\sigma_1^2} \\ \frac{1}{\sigma_1}^2 & \frac{1}{\sigma_1^2} \end{pmatrix} \tag{B.4}$$

We then get the covariance by inverting this, yielding

$$\begin{pmatrix} \sigma_2^2 & -\sigma_2^2 \\ -\sigma_2^2 & \sigma_1^2 + \sigma_2^2 \end{pmatrix} \tag{B.5}$$

We can simply generalize this for large numbers of parameters, but at that point it would be better to do so computationally.

Now, say we assume that we have a Gaussian prior with width σ, we can add these to the appropriate diagonal element of the Fisher matrix, via

$$F_{kl} \to F_{kl} + \frac{\delta_{kl}\delta_{il}}{\sigma^2} \tag{B.6}$$

In the case if the prior is not a single parameter in the Fisher matrix, we transform it to where it is, then transform the now diagonal Fisher matrix prior into the working variables.

Now that we have gone over the formalism, let's talk about how we use this in practice. First, Fisher matrix works under the assumption that the parameter space that is being probed is close to some fiducial values. Another thing that we may need to do is make a Fisher matrix over a smaller parameter space by marginalizing over nuisance parameters. We can do this by integrating over those parameters without assuming a prior. Simply, invert F, then remove rows and columns marginalized over, then invert F again.

Another practical aspect of Fisher matrices is that if we have two independent data sets A and B, we can find the Fisher matrix for the combined distribution by simply adding the two. Note that any marginalization must be done after the summation of the two Fisher matrices. You can marginalize prior to it if the two sets have disjoint nuisance parameters.

References

Abazajian K. N., et al., 2009, The Astrophysical Journal Supplement Series, 182, 543

Abazajian K. N., et al., 2016, CMB-S4 Science Book, First Edition (arXiv:1610.02743)

Adam R., et al., 2017, Astronomy & Astrophysics, 598, A115

Adam R., et al., 2018, Astronomy & Astrophysics, 609, A115

Ade P., et al., 2013, Astronomy & Astrophysics, 554, A140

Ade P., et al., 2016a, Astronomy & Astrophysics, 586, A140

Ade P., et al., 2016b, Astronomy & Astrophysics, 594, A27

Ade P., et al., 2019, Journal of Cosmology and Astroparticle Physics, 2019, 056–056

Aghanim N., et al., 2016a, Astronomy & Astrophysics, 594, A11

Aghanim N., et al., 2016b, Astronomy & Astrophysics, 594, A22

Ahn C. P., et al., 2012, The Astrophysical Journal Supplement Series, 203, 21

Ahn C. P., et al., 2014, The Astrophysical Journal Supplement Series, 211, 17

Albrecht A., et al., 2006, Report of the Dark Energy Task Force (arXiv:astro-ph/0609591)

Allen S. W., Schmidt R., Fabian A., 2001, Monthly Notices of the Royal Astronomical Society, 328, L37

Arnaud M., Pratt G., Piffaretti R., B´ohringer H., Croston J., Pointecouteau E., 2010, Astronomy & Astrophysics, 517, A92

Battaglia N., Natarajan A., Trac H., Cen R., Loeb A., 2013, The Astrophysical Journal, 776, 83

Battaglia N., et al., 2019, Probing Feedback in Galaxy Formation with Millimeter-wave Observations (arXiv:1903.04647)

Benson B. A., et al., 2014, Millimeter, Submillimeter, and Far-Infrared Detectors and Instrumentation for Astronomy VII

Bernardis F. D., et al., 2017, Journal of Cosmology and Astroparticle Physics, 2017, 008–008

Bertoldi F., 2018, The Atacama Large Aperture Submm/mm Telescope (AtLAST) Project, doi:10.5281/zenodo.1158842, https://doi.org/10.5281/zenodo.1158842

Birkinshaw M., Hughes J., 1994, The Astrophysical Journal, 420, 33

Birkinshaw M., Gull S. F., Northover K. J. E., 1978, Nature, 275, 40,41

Birkinshaw M., Gull S. F., Hardebeck H., 1984, Nature, 309, 34

Bregman J. N., Otte B., Irwin J. A., Putman M. E., Lloyd-Davies E. J., Brüns C., 2009, The Astrophysical Journal, 699, 1765

Bryan S., et al., 2018, in Millimeter, Submillimeter, and Far-Infrared Detectors and Instrumentation for Astronomy IX. p. 107080J

Burles S., Tytler D., 1998, The Astrophysical Journal, 499, 699

Burles S., Nollett K. M., Turner M. S., 2001, The Astrophysical Journal Letters, 552, L1

Calafut V., Bean R., Yu B., 2017, Physical Review D, 96

Carlstrom J. E., Joy M., Grego L., 1996, The Astrophysical Journal Letters, 456, L75

Carlstrom J. E., Holder G. P., Reese E. D., 2002, Annual Review of Astronomy and Astrophysics, 40, 643–680

Carlstrom J., et al., 2011, Publications of the Astronomical Society of the Pacific, 123, 568

Cen R., Ostriker J. P., 2006, The Astrophysical Journal, 650, 560

Cole S., Kaiser N., 1988, Monthly Notices of the Royal Astronomical Society, 233, 637

Cooray A., Chen X., 2002, The Astrophysical Journal, 573, 43

Croton D. J., et al., 2006, Monthly Notices of the Royal Astronomical Society, 365, 11–28

DeDeo S., Spergel D. N., Trac H., 2005, The kinetic Sunyaev-Zel'dovitch effect as a dark energy probe (arXiv:astro-ph/0511060)

Delabrouille J., et al., 2018, Journal of Cosmology and Astroparticle Physics, 2018, 014–014

Désert F.-X., et al., 1998, New Astronomy, 3, 655

Dicker S., et al., 2008, in Millimeter and Submillimeter Detectors and Instrumentation for Astronomy IV. p. 702005

Dicker S., et al., 2014, Journal of Low Temperature Physics, 176, 808

Erler J., Basu K., Chluba J., Bertoldi F., 2018, Monthly Notices of the Royal Astronomical Society, 476, 3360–3381

Ferraro S., Hill J. C., Battaglia N., Liu J., Spergel D. N., 2016, Physical Review D, 94

Ferreira P. G., Juszkiewicz R., Feldman H. A., Davis M., Jaffe A. H., 1999, The Astrophysical Journal, 515, L1

Flender S., Bleem L., Finkel H., Habib S., Heitmann K., Holder G., 2016, The Astrophysical Journal, 823, 98

Font-Ribera A., et al., 2013, Journal of Cosmology and Astroparticle Physics, 2013, 018–018

Gull S., Northover K., 1976, Nature, 263, 572

Hand N., et al., 2012, Physical Review Letters, 109, 041101

Hasselfield M., et al., 2013, Journal of Cosmology and Astroparticle Physics, 2013, 008

Henderson S. W., et al., 2016, Journal of Low Temperature Physics, 184, 772–779

Hill J. C., Ferraro S., Battaglia N., Liu J., Spergel D. N., 2016, Physical Review Letters, 117

Hurier G., 2016, Astronomy & Astrophysics, 596, A61

Ivezić , et al., 2019, The Astrophysical Journal, 873, 111

Jones M., et al., 1993, Nature, 365, 320

Keisler R., Schmidt F., 2013, The Astrophysical Journal Letters, 765, L32

Kilbinger M., 2015, Reports on Progress in Physics, 78, 086901

Kitayama T., et al., 2016, Publications of the Astronomical Society of Japan, 68, 88

Komatsu E., Seljak U., 2002, Monthly Notices of the Royal Astronomical Society, 336, 1256

Komatsu E., Kitayama T., Suto Y., Hattori M., Kawabe R., Matsuo H., Schindler S., Yoshikawa K., 1999, The Astrophysical Journal Letters, 516, L1

Komatsu E., et al., 2001, Publications of the Astronomical Society of Japan, 53, 57

Korngut P., et al., 2011, The Astrophysical Journal, 734, 10

Lamarre J., et al., 1998, The Astrophysical Journal Letters, 507, L5

Lin K.-Y., et al., 2009, The Astrophysical Journal, 694, 1629

Markevitch M., Vikhlinin A., 2007, Physics Reports, 443, 1

Mason B., et al., 2010, The Astrophysical Journal, 716, 739

McCarthy I. G., et al., 2007, Monthly Notices of the Royal Astronomical Society, 376, 497

Menanteau F., et al., 2010, The Astrophysical Journal, 723, 1523

Moffet A. T., Birkinshaw M., 1989, Astronomical Journal, 98, 1148

Mroczkowski T., et al., 2012, The Astrophysical Journal, 761, 47

Mroczkowski T., et al., 2019a, A High-resolution SZ View of the Warm-Hot Universe (arXiv:1903.02595)

Mroczkowski T., et al., 2019b, Space Science Reviews, 215

Muchovej S., et al., 2007, The Astrophysical Journal, 663, 708

Mueller E.-M., De Bernardis F., Bean R., Niemack M. D., 2015a, Physical Review D, 92, 063501

Mueller E.-M., Bernardis F. d., Bean R., Niemack M. D., 2015b, The Astrophysical Journal, 808, 47

Nagai D., Kravtsov A. V., Kosowsky A., 2003, The Astrophysical Journal, 587, 524

Nicastro F., Mathur S., Elvis M., 2008, Science, 319, 55

Nord M., et al., 2009, Astronomy & Astrophysics, 506, 623

Padin S., 2014, Appl. Opt., 53, 4431

Penzias A. A., Wilson R. W., 1965, Astrophys. J., 142, 419

Perlmutter S., et al., 1999, The Astrophysical Journal, 517, 565

Pointecouteau E., Giard M., Benoit A., Désert F., Aghanim N., Coron N., Lamarre J., Delabrouille J., 1999, The Astrophysical Journal Letters, 519, L115

Pryke C., Halverson N., Leitch E., Kovac J., Carlstrom J., Holzapfel W., Dragovan M., 2002, The Astrophysical Journal, 568, 46

Reese E. D., et al., 2000, The Astrophysical Journal, 533, 38

Reese E. D., Carlstrom J. E., Joy M., Mohr J. J., Grego L., Holzapfel W. L., 2002, The Astrophysical Journal, 581, 53

Remazeilles M., Bolliet B., Rotti A., Chluba J., 2018, Monthly Notices of the Royal Astronomical Society, 483, 3459–3464

Richard Thompson A., Moran J. M., Swenson Jr G. W., 2017, Interferometry and synthesis in radio astronomy. Springer Nature

Ruan J. J., Quinn T. R., Babul A., 2013, Monthly Notices of the Royal Astronomical Society, 432, 3508–3519

Sayers J., et al., 2013, The Astrophysical Journal, 778, 52

Schaan E., et al., 2015, arXiv preprint arXiv:1510.06442

Schwan D., et al., 2003, New Astronomy Reviews, 47, 933

Sehgal N., Kosowsky A., Holder G., 2005, The Astrophysical Journal, 635, 22

Shaw L. D., Nagai D., Bhattacharya S., Lau E. T., 2010, The Astrophysical Journal, 725, 1452

Shull J. M., Smith B. D., Danforth C. W., 2012, The Astrophysical Journal, 759, 23

Smirnov A., et al., 2012, in Space Telescopes and Instrumentation 2012: Optical, Infrared, and Millimeter Wave. p. 84424C

Soergel B., et al., 2016, Monthly Notices of the Royal Astronomical Society, 461, 3172

Stacey G., et al., 2018, in Ground-based and Airborne Telescopes VII. p. 107001M

Staniszewski Z., et al., 2009, The Astrophysical Journal, 701, 32

Sunyaev R. A., Zeldovich Y. B., 1970, Astrophysics and Space Science, 7, 3

Sunyaev R., Zeldovich Y. B., 1972, Comments on Astrophysics and Space Physics, 4, 173

Sunyaev R. A., Zeldovich I. B., 1980, Monthly Notices of the Royal Astronomical Society, 190, 413

Sunyaev R. A., Norman M. L., Bryan G. L., 2003, Astronomy Letters, 29, 783

Sutin B., et al., 2018, PICO - the probe of inflation and cosmic origins (arXiv:1808.01368)

Tanimura H., et al., 2019, Monthly Notices of the Royal Astronomical Society, 483, 223

White S. D., Navarro J. F., Evrard A. E., Frenk C. S., 1993, nature, 366, 429

Wilbanks T., Ade P., Fischer M., Holzapfel W., Lange A., 1994, The Astrophysical Journal, 427, L75

Wittman D., 20xx, Fisher Matrix for Beginners

Zemcov M., Borys C., Halpern M., Mauskopf P., Scott D., 2007, Monthly Notices of the Royal Astronomical Society, 376, 1073

Zemcov M., et al., 2010, Astronomy & Astrophysics, 518, L16

Zemcov M., et al., 2012, The Astrophysical Journal, 749, 114

de Graaff A., Cai Y.-C., Heymans C., Peacock J. A., 2019, Astronomy $&$ Astrophysics, 624, A48